Image-domain wavefield tomography for tilted transversely isotropic media

Vladimir Li[1]*, Ilya Tsvankin[1], Antoine Guitton[1,2] and Hui Wang[3]

[1]*Center for Wave Phenomena, Colorado School of Mines, 1500 Illinois St., Golden, CO 80401, USA,* [2]*Total CSTJF, EC465, Avenue Larribau, Pau, 64018 PAU Cedex, France, and* [3]*CGG, 10300 Town Park Dr, Houston, TX 77072, USA*

ABSTRACT

Transversely isotropic models with a tilted symmetry axis have become standard for imaging beneath dipping shale formations and in active tectonic areas. Here, we develop a methodology of wave-equation-based image-domain tomography for acoustic tilted transversely isotropic media. We obtain the gradients of the objective function using an integral wave-equation operator based on a separable dispersion relation that takes the symmetry-axis tilt into account. In contrast to the more conventional differential solutions, the integral operator produces only the P-wavefield without shear-wave artefacts, which facilitates both imaging and velocity analysis. The model is parameterized by the P-wave zero-dip normal-moveout velocity, the Thomsen parameter δ, anellipticity coefficient η and the symmetry-axis tilt θ. Assuming that the symmetry axis is orthogonal to reflectors, we study the influence of parameter errors on energy focusing in extended (space-lag) common-image gathers. Distortions in the anellipticity coefficient η introduce weak linear defocusing regardless of reflector dip, whereas δ influences both the energy focusing and depth scale of the migrated section. These results, which are consistent with the properties of the P-wave time-domain reflection moveout in tilted transversely isotropic media, provide important insights for implementation of velocity model-building in the image-domain. Then the algorithm is tested on a modified anticline section of the BP 2007 benchmark model.

Key words: Wave equation, TTI media, Tomography.

INTRODUCTION

Transversely isotropic (TI) models are widely used for processing and inversion of reflection data. For complex geologic environments (e.g. subsalt plays, fold-and-thrust belts and fault zones), it is essential to properly account for the tilt of the symmetry axis. However, most existing tilted TI (TTI) velocity-analysis algorithms are based on ray-theory techniques such as Kirchhoff migration (e.g. Wang and Tsvankin 2013a,b) and may not be sufficiently robust in the presence of strong heterogeneity.

Image-domain tomography (IDT) operates with the output of wave-equation migration and updates velocity models using energy focusing in the extended domain. Application of reverse-time migration (RTM) allows IDT algorithms to properly handle structurally complex models. Current implementations of IDT (Y. Li *et al.* 2016; V. Li *et al.* 2017a) are limited to TI media with a vertical symmetry axis (VTI). Weibull and Arntsen (2014) present an IDT algorithm based on the TTI elastic wave equation but their imaging condition employs a purely isotropic wave-mode decomposition technique. Also, although elastic extended images can provide more accurate amplitudes compared to their acoustic counterparts, they are still contaminated by aperture-truncation artefacts (Li *et al.* 2018) that need to be mitigated prior to back-projecting the image residuals.

*E-mail: vli@alumni.mines.edu

Here, we extend to tilted transverse isotropy the VTI IDT algorithm developed by Li *et al.* (2018), which requires addressing the following issues:

- wavefield extrapolation;
- computation of the gradient of the objective function;
- analysis of the sensitivity of the objective function to the TTI parameters.

In principle, wavefield extrapolation for IDT purposes can be carried out with elastic wave-equation operators. However, in addition to the high cost of elastic modelling, it requires either developing a suitable elastic imaging condition or employing expensive and often unreliable mode-decomposition techniques. A more practical alternative is to use acoustic wave-equation operators (Alkhalifah 1998) based on either differential or integral wave-equation solutions. The latter approach employs the dispersion relation to compute phase shifts needed for time-stepping the wavefield (Du, Fowler and Fletcher 2014) and allows one to extrapolate the P-wavefront without the so-called shear-wave artefacts (Grechka, Zhang and Rector 2004).

Integral operators can be implemented by employing either the low-rank approximation or a separable form of the dispersion relation. A comparative review of anisotropic acoustic operators can be found in Du, Fowler and Fletcher (2014). Here, we use the 'strongly anelliptic' (i.e. valid for large absolute values of the anellipticity parameter η) separable dispersion relation derived by Schleicher and Costa (2016). Following Zhan, Pestana and Stoffa (2012), we obtain the separable TTI formulation by applying the wavenumber rotation to the VTI equation.

The main challenge in anisotropic velocity model-building is the trade-off between the medium parameters. Analysis of the parameter signatures can provide useful insights into model updating and help design a suitable inversion strategy. The extended-domain signatures of the zero-dip normal-moveout (NMO) velocity $V_{nmo}(0)$, δ and η are related to their influence on the conventional-spread and non-hyperbolic moveout. Sava and Alkhalifah (2012) and Li, Tsvankin and Alkhalifah (2016) demonstrate that for VTI media the contribution of η increases with reflector dip (because η influences the NMO velocity of dipping events) and that energy focusing in the extended domain is sensitive to the lateral variation of δ (but not to δ itself). However, in TTI media with the symmetry axis orthogonal to interfaces, the NMO velocity is determined by $V_{nmo}(0)$ and δ, with no contribution of η (Tsvankin and Grechka 2011).

Here, we present an RTM-based IDT algorithm for two-dimensional acoustic TTI media. We start by introducing a separable dispersion relation for strongly anelliptic TTI models, which is employed in wavefield extrapolation and in the derivation of the inversion gradients. A review of the properties of the NMO velocity in TTI media helps explain the design of the inversion methodology. Then, using a homogeneous TTI model with a dipping interface, we discuss how the known properties of reflection moveout translate to the extended domain. Next, we test the obtained gradient expressions and evaluate the influence of the symmetry-axis tilt on the inversion gradients. Finally, the developed IDT algorithm is applied to synthetic data from a modified anticline segment of the BP 2007 benchmark model.

THEORY

Wavefield extrapolation operator

The dispersion relation for tilted transversely isotropic (TTI) models with the symmetry axis in the $[x, z]$-plane can be obtained by applying a wavenumber rotation to the corresponding VTI expression (Schleicher and Costa 2016) that includes linear and quadratic terms in the anisotropy coefficients:

$$\omega^2 = V_{nmo}^2(0)\,\hat{k}_x^2 + \frac{V_{nmo}^2(0)}{1 + 2\delta}\,\hat{k}_z^2 + 2\eta\,V_{nmo}^2(0)\,\frac{\hat{k}_x^4}{\hat{k}_x^2 + \hat{k}_z^2}$$
$$+ 4V_{nmo}^2(0)\,\eta\,\varepsilon\,\frac{\hat{k}_x^4\,\hat{k}_z^2}{(\hat{k}_x^2 + \hat{k}_z^2)^2}$$
$$+ 4V_{nmo}^2(0)\,\eta\,(\varepsilon - \delta)\,\frac{\hat{k}_x^4\,\hat{k}_z^4}{(\hat{k}_x^2 + \hat{k}_z^2)^3}, \tag{1}$$

$$\begin{bmatrix} \hat{k}_x \\ \hat{k}_z \end{bmatrix} = \begin{bmatrix} \cos\theta & \sin\theta \\ -\sin\theta & \cos\theta \end{bmatrix} \begin{bmatrix} k_x \\ k_z \end{bmatrix},$$

where k_x and k_z are the horizontal and vertical wavenumbers, $\hat{k}_x$ and $\hat{k}_z$ are the corresponding wavenumbers in the rotated coordinate system and θ is the tilt of the symmetry axis. The Padé coefficients q_1 and q_2 in equation (65) of Schleicher and Costa (2016) are set to 0.5 and 0.25, respectively; their coefficient g is set to unity, which means that the shear-wave velocity in the symmetry-axis direction is equal to zero.

Implementation of the dispersion relation (equation (1)) in wavefield extrapolation requires separating the tilt θ from the wavenumber components. Zhan, Pestana and Stoffa (2012) derive a linearized separable approximation that contains only the three leading terms of equation (1). Although being sufficiently accurate for weakly anisotropic TTI media and possibly suitable for deriving image-domain
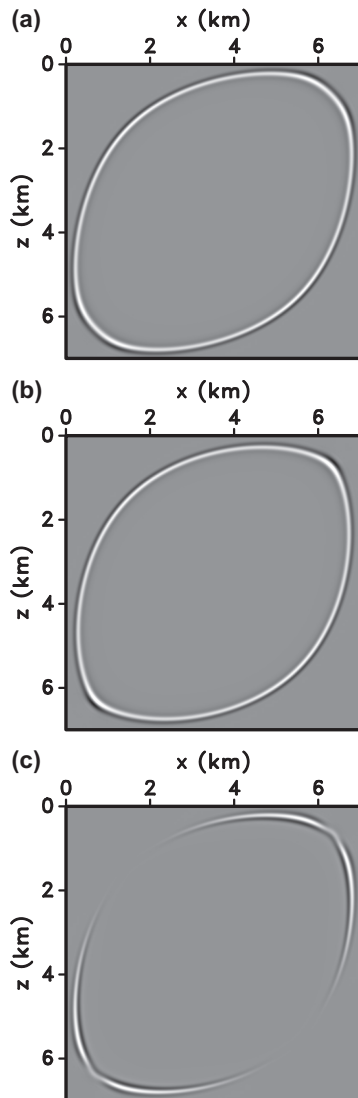
Figure 1 P-wavefront in a homogeneous TTI medium computed using (a) the 'strongly anelliptic' dispersion relation (equation (A2)) and (b) the 'weakly anelliptic' approximation (equation (A1)). (c) The difference between the wavefronts on plots (a) and (b).

tomography gradients, this approximation can be improved by retaining the entire dispersion relation in equation 1 (see the Appendix). Separable formulations of equation (1) for weakly and strongly anisotropic TTI media (equations (A1) and (A2), respectively) are obtained by collecting all terms with the same wavenumber components.

Figure 1 shows that even for TTI media with moderate anisotropy coefficients ($\delta = 0.1$, $\eta = 0.15$), equation (A2) produces a more accurate wavefront at oblique angles with the symmetry axis than the linearized approximation (equation (A1)).

Image-domain tomography gradients

The gradients of the objective function for image-domain tomography (IDT) or full-waveform inversion can be efficiently computed using the adjoint-state method (Plessix 2006). The quality of focusing in extended images is typically evaluated with the differential semblance optimization (DSO) (Symes and Carazzone 1991) or image-power (IP) operators (Chavent and Jacewitz 1995; Zhang and Shan 2013). The general sequence of steps for deriving the IDT gradients in VTI media is described in Li *et al.* (2017b). Here, we extend their results to TTI models parameterized by $V_{nmo}(0)$, δ, η and the symmetry-axis tilt θ. Note that the expressions for the inversion gradients are valid for arbitrary orientation of the symmetry axis. The gradients listed below are obtained directly from equation (1) rather than its more complex separable form, which significantly facilitates the derivation:

$$
\left[\frac{\partial \mathcal{J}}{\partial \mathbf{m}} \right]_i = \begin{bmatrix} \dfrac{\partial \mathcal{J}}{\partial \delta} \\[6pt] \dfrac{\partial \mathcal{J}}{\partial V_{nmo}(0)} \\[6pt] \dfrac{\partial \mathcal{J}}{\partial \eta} \\[6pt] \dfrac{\partial \mathcal{J}}{\partial \theta} \end{bmatrix}_i = -\sum_{e,\tau} \delta(\tau)
$$

$$
\times \begin{bmatrix} -\dfrac{2 V_{nmo}^2(0)}{(1+2\delta)^2} & 0 & 0 & 0 \\[6pt] 0 & 2V_{nmo}(0) & 0 & 0 \\[6pt] 0 & 0 & 2V_{nmo}^2(0) & 0 \\[6pt] 0 & 0 & 0 & 2V_{nmo}^2(0) \end{bmatrix} \begin{bmatrix} f_1 \\ f_2 \\ f_3 \\ f_4 \end{bmatrix},
$$

$$
f_1 = \left[(k_z \cos\theta - k_x \sin\theta)^2 \, u_i \right] \star a_i \,,
$$

$$
f_2 = \left[\left((k_x \cos\theta + k_z \sin\theta)^2 + \frac{(k_z \cos\theta - k_x \sin\theta)^2}{1+2\delta} \right. \right.
$$
$$
\left. \left. + 2\eta \frac{(k_x \cos\theta + k_z \sin\theta)^4}{k_x^2 + k_z^2} \right) u_i \right] \star a_i \,,
$$

$$
f_3 = \left[\frac{(k_x \cos\theta + k_z \sin\theta)^4}{k_x^2 + k_z^2} \, u_i \right] \star a_i \,,
$$

$$
f_4 = \left[(k_z \cos\theta - k_x \sin\theta) \left(k_x \cos\theta + k_z \sin\theta - \frac{k_x \cos\theta + k_z \sin\theta}{1+2\delta} \right. \right.
$$
$$
\left. \left. + 4\eta \frac{(k_x \cos\theta + k_z \sin\theta)^3}{k_x^2 + k_z^2} \right) u_i \right] \star a_i \,, \quad i = s, r \,, \tag{2}
$$

where $\mathcal{J}$ is the IDT objective function, $\mathbf{m}$ is the model-parameter vector, τ is the correlation lag, e is the experiment (shot) index, $\delta(\tau)$ is the Dirac delta function, '$\star$' denotes cross-correlation, u_i and a_i are the forward and adjoint wavefields, respectively and i denotes the source (s) or receiver (r) side.

The only difference between the gradients of the DSO and IP objective functions is in the adjoint wavefields a_i that are computed using the corresponding penalty functions. If the symmetry axis is vertical ($\theta = 0°$), equation (2) reduces to the VTI form presented by Li *et al.* (2017b).

P-wave normal-moveout velocity for tilted transverse isotropy

The extended-domain signatures of the TTI parameters play a key role in the sensitivity analysis and can help in optimizing the inversion strategy. Those signatures are governed by the properties of P-wave reflection moveout in the time domain. For a homogeneous TTI medium with the symmetry axis orthogonal to the reflector, the exact P-wave normal-moveout (NMO) velocity is given by (Tsvankin 2012):

$$V_{\text{nmo}}(\theta) = \frac{V_{\text{nmo}}(0)}{\cos\theta} = \frac{V_{\text{nmo}}(0)}{\sqrt{1 - p^2 V_{P0}^2}},$$

$$V_{\text{nmo}}(0) = V_{P0}\sqrt{1 + 2\delta},$$

$$p = \frac{\sin\theta}{V_{P0}}, \tag{3}$$

where V_{P0} is the P-wave symmetry-direction velocity and p is the horizontal slowness (ray parameter) of the zero-offset ray. Note that p (unlike θ) can be determined from P-wave reflection traveltimes because it is equal to the time slope on the zero-offset (or stacked) section. Hence, it is possible to estimate both V_{P0} and δ if $V_{\text{nmo}}(0)$ can be obtained from horizontal events (e.g. for a bending TTI layer; see Tsvankin and Grechka 2011). However, if the TTI parameters vary laterally, NMO-velocity inversion cannot be performed without additional information.

Equation (3) shows that, in contrast to VTI media, η does not influence the P-wave NMO velocity regardless of reflector dip. Therefore, errors in η will only influence non-hyperbolic moveout and imaging of far-offset data (Tsvankin and Grechka 2011). The parameter δ, however, does contribute to $V_{\text{nmo}}(p)$, if the medium is parameterized by $V_{\text{nmo}}(0)$, δ and η. This means that δ-errors in TTI media should cause not only a depth shift in the migrated domain but also defocusing in extended images, which is confirmed by the synthetic tests.

METHODOLOGY

Wavefield extrapolation is performed with the integral operator based on the dispersion relation in equation (A2), which is valid for strongly anelliptic media. Similarly to Li *et al.* (2018), parameter updating is carried out by focusing energy in extended least-squares reverse-time migration (LSRTM) images. Application of LSRTM helps reduce kinematic artefacts in the extended domain and improve the robustness of model updating. As a linear inverse problem, LSRTM can be efficiently implemented using a conjugate-direction algorithm (Claerbout 1992). The convergence of LSRTM can be expedited by applying non-stationary matching filters to the LSRTM gradient (Guitton 2017; Li *et al.* 2018). The matching filters approximate the inverse Hessian of the data-misfit objective function and produce so-called 'pseudoinverse' images.

Extension of the algorithm described in Li *et al.* (2017a) to tilted transverse isotropy requires adjustments in the objective function and inversion strategy. For dipping events in TTI models, the normal-moveout (NMO) velocity is controlled by its zero-dip value $V_{\text{nmo}}(0)$ and δ. However, especially in the presence of lateral heterogeneity, it is not feasible to reliably constrain both $V_{\text{nmo}}(0)$ and δ from only P-wave reflection traveltimes. Therefore, we incorporate vertical δ-profiles at available boreholes into the image-domain objective function (Li *et al.* 2018) as follows:

$$\mathcal{J} = (1 - \beta)(\mathcal{J}_{\text{DSO}} - \alpha\,\mathcal{J}_{\text{IP}}) + \beta\,||\delta - \delta_{\text{ref}}||, \tag{4}$$

where δ_{ref} is the reference δ-field obtained from image-guided interpolation between the boreholes, and α and β are model-dependent weighting factors. To steer the algorithm towards geologically plausible solutions, image-guided smoothing (Hale 2009; Wang and Tsvankin 2013b) is applied to the inversion gradients. Model updating is carried out by the L-BFGS inversion algorithm. The symmetry axis is assumed to be orthogonal to reflectors, and its tilt is found from the interface dips in the LSRTM images.

Because $V_{\text{nmo}}(0)$ and δ influence the NMO velocity in TTI media, these parameters can be constrained prior to updating η (hereafter, for brevity we denote $V_{\text{nmo}}(0)$ simply as V_{nmo}). Therefore, parameter estimation can be performed sequentially by first fitting conventional-spread moveout (via updates in V_{nmo} and δ) and then non-hyperbolic moveout (via updates in η). This sequence (see also Wang and Tsvankin 2013b; Pattnaik *et al.* 2016) is repeated until further iterations no longer reduce the objective function.

SIGNATURES OF MEDIUM PARAMETERS

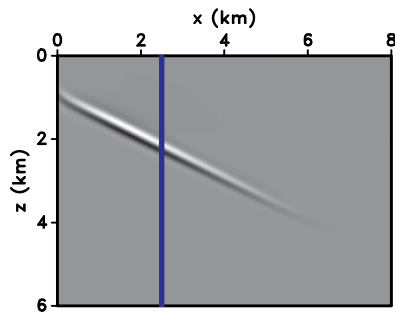We analyse the parameter signatures in the extended domain for a reflector dipping at $30°$ beneath a homogeneous

Figure 2 Conventional RTM image for a model with a dipping reflector beneath a homogeneous TTI medium ($V_{nmo} = 2.7$ km/s, $\eta = \delta = 0.15$; the symmetry axis is orthogonal to the reflector). The vertical blue line marks the location of the common-image gather (CIG) displayed in Figs. 3– 6.
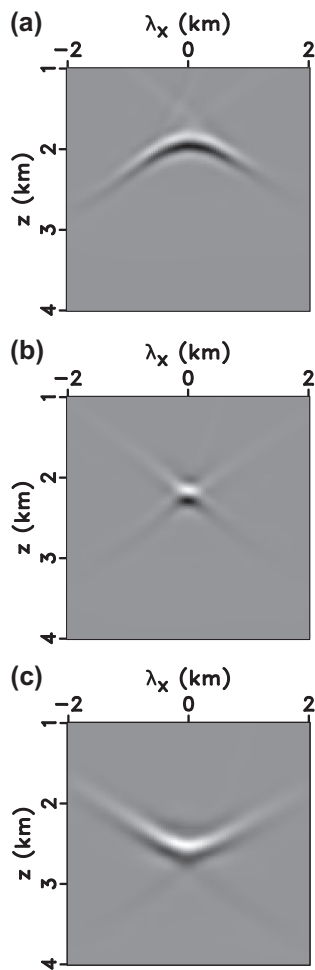

Figure 3 Space-lag CIGs for the model in Fig. 2 computed with: (a) $V_{nmo} = 2.4$ km/s, (b) $V_{nmo} = 2.7$ km/s (actual value) and (c) $V_{nmo} = 3.0$ km/s. The parameters δ and η are kept at their actual values.
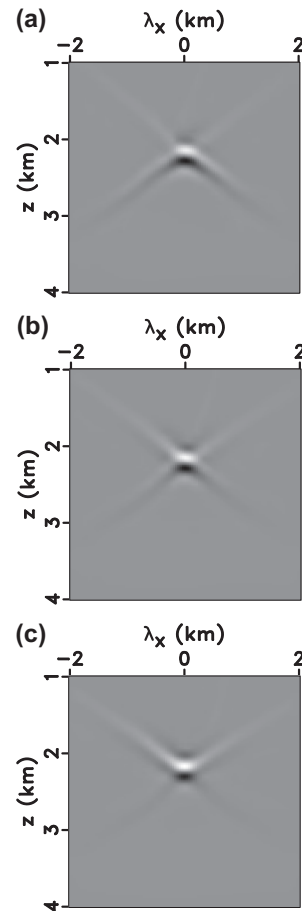
Figure 4 Space-lag CIGs for the model in Fig. 2 computed with: (a) $\eta = 0$, (b) $\eta = 0.15$ (actual value) and (c) $\eta = 0.3$.

tilted tranversely isotropic (TTI) medium; the symmetry axis is orthogonal to the reflector. The model parameters are defined on a rectangular grid, and the data are generated by 51 sources evenly spaced at the surface. The conventional reverse-time-migration (RTM) image computed with the actual model is shown in Fig. 2. Application of non-stationary matching filters suppresses the kinematic artefacts caused by aperture truncation and increases the sensitivity of energy focusing to the TTI parameters. Space-lag common-image gathers (CIGs) are generated at surface location 2.5 km for a representative range of the parameters V_{nmo}, η and δ. We distort one parameter at a time, keeping the remaining two parameters at their actual values.

The gathers computed with V_{nmo} distorted by about ±11% show visible defocusing (Fig. 3), which is similar to the signature of this parameter in isotropic and VTI media. Errors in η produce residual energy (Fig. 4) that has a linear (V-like) shape that was also observed in extended images
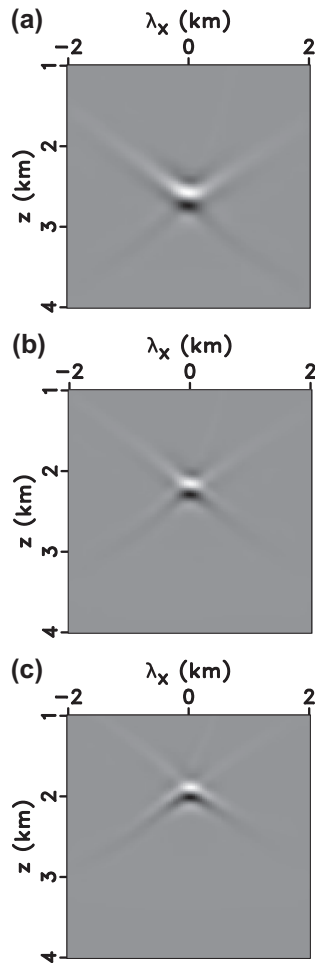
Figure 5 Space-lag CIGs for the model in Fig. 2 computed with: (a) $\delta = 0$, (b) $\delta = 0.15$ (actual value) and (c) $\delta = 0.3$.
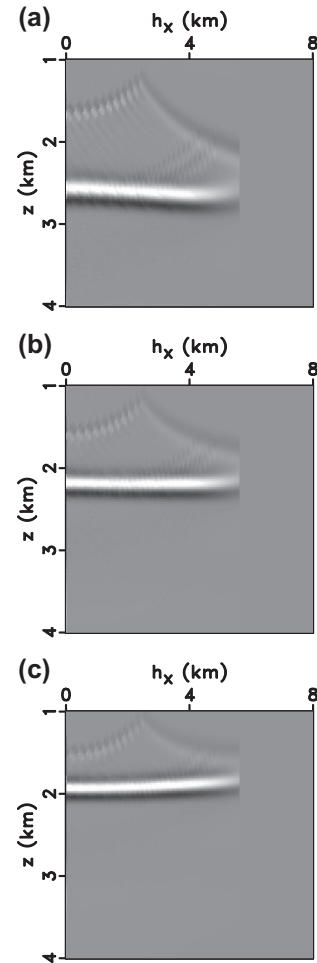
Figure 6 Surface-offset CIGs computed with Kirchhoff migration for the model in Fig. 2 using (a) $\delta = 0$, (b) $\delta = 0.15$ (actual value) and (c) $\delta = 0.3$; h_x is the half-offset.

generated with inaccurate η-values for near-horizontal interfaces in VTI media (Sava and Alkhalifah 2012; Li *et al.* 2016). This is explained by the fact that in both cases η influences only non-hyperbolic (long-spread) moveout.

Distortions in the δ-field lead to both depth shifts and moderate defocusing, with the latter caused by the influence of that parameter on the normal-moveout velocity of dipping events (Fig. 5, see equation (3)). To confirm our interpretation of the extended-domain signatures, we also use Kirchhoff migration to compute surface-offset CIGs, which clearly show the residual moveout caused by errors in δ (Fig. 6).

GRADIENT COMPUTATION

Next, we compute the η-gradient in the image domain for the model in Fig. 2. To evaluate the influence of the

symmetry-axis tilt, we compare the differential semblance optimization (DSO) and image-power (IP) gradients obtained from the tilted transversely isotropic (TTI) (Fig. 7) and VTI (Fig. 8) equations.

For both the DSO (compare Fig. 7a,b with Fig. 8a,b) and IP (compare Fig. 7c,d with Fig. 8c,d) operators, there is a noticeable difference between the results for a vertical and tilted symmetry axis. This confirms that neglecting the tilt should introduce significant distortions in parameter estimation for dipping interfaces beneath TTI media (Behera and Tsvankin 2009; Wang and Tsvankin 2013a, 2013b). Note that the gradients (especially, that for DSO) suffer from the aperture-truncation artefacts in the extended images, as mentioned above. These kinematic artefacts need to be mitigated (e.g., by least-squares reverse-time migration) prior
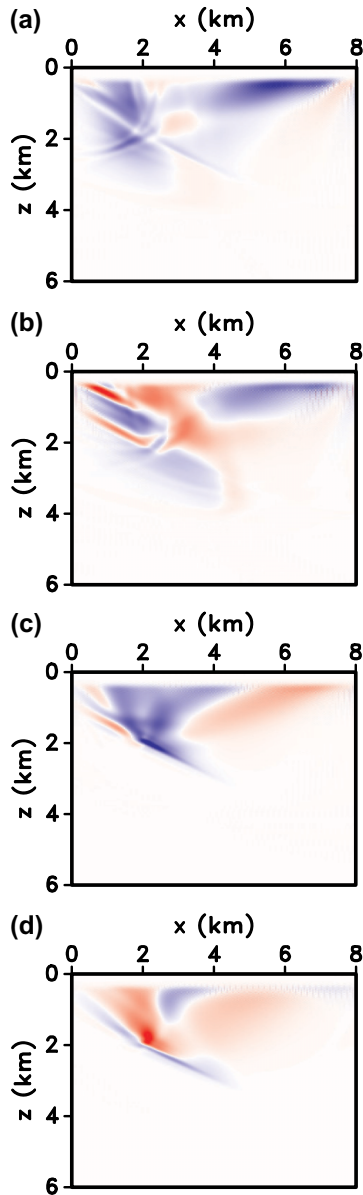
(a)

(b)

(c)

(d)

Figure 7 IDT gradients for the model in Fig. 2 computed from the TTI equations with the DSO (a,b) and IP (c,d) operators. Plots (a,c) are obtained with the understated $\eta = 0$. Plots (b,d) are obtained with the overstated $\eta = 0.3$.

(a)

(b)

(c)

(d)

Figure 8 IDT gradients for the model in Fig. 2 computed from the VTI equations with the DSO (a,b) and IP (c,d) operators. Plots (a,c) are obtained with the understated $\eta = 0$. Plots (b,d) are obtained with the overstated $\eta = 0.3$.

to back-projecting the image residuals for model-updating purposes.

TEST ON BP MODEL

The inversion methodology described above is applied to synthetic data from a modified anticline segment of the BP 2007 model. The dep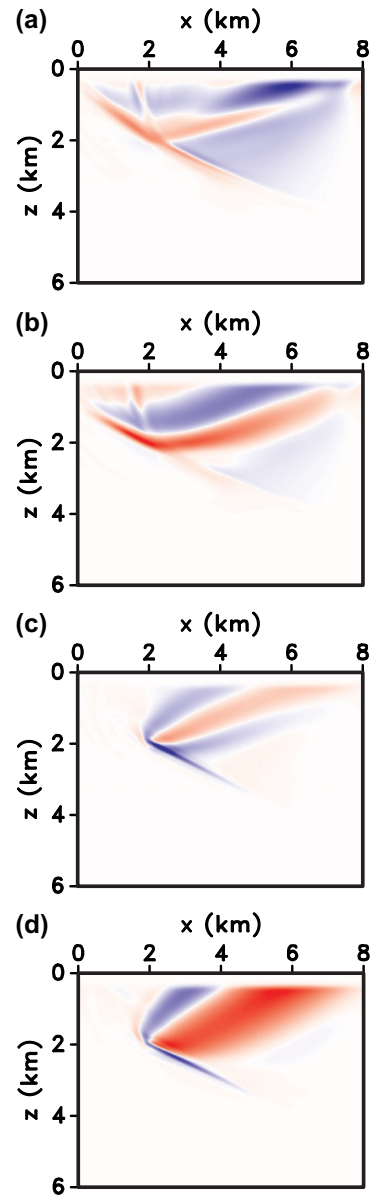th scale of the original model is squeezed by a factor of two, which reduces the symmetry-axis tilt by approximately the same factor. The data for the BP model are recomputed with our acoustic wavefield simulator and include 120 'streamer' arrays with the maximum offset of 6 km.

The initial model is elliptic and laterally invariant (1D). It is obtained by interpolating the left-most profile of the actual V_{nmo}-field (Fig. 9) over the entire section. We assume that δ is known at a single borehole location ($x = 18.5$ km), and
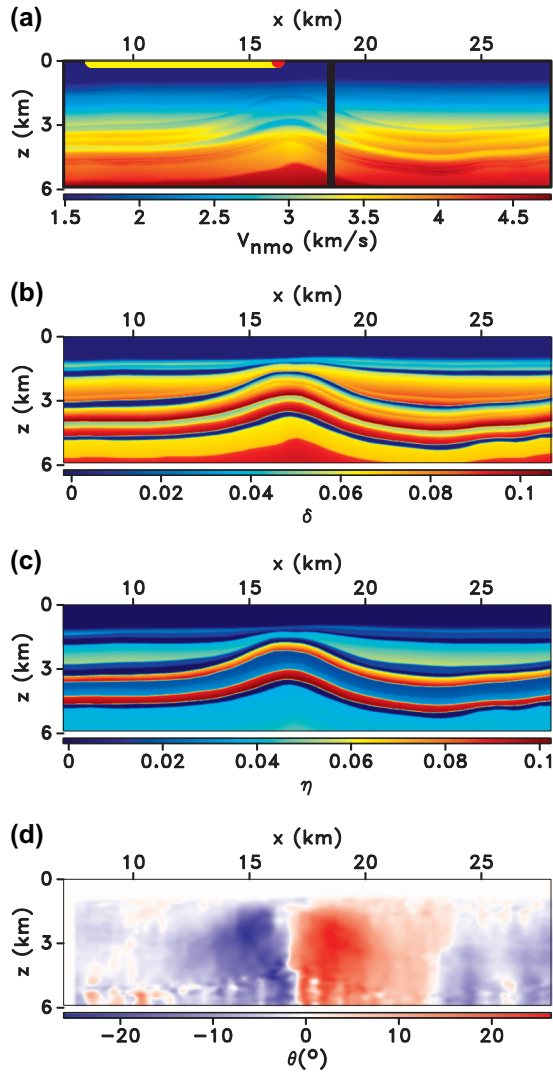
Figure 9 Parameters of the modified BP model: (a) V_{nmo}, (b) δ, (c) η and (d) tilt θ (the symmetry axis is orthogonal to the reflectors). The vertical black line on plot (a) marks the 'borehole' location where a δ-profile is available. A total of 120 sources (one of them is marked by a red dot) are evenly spaced at the surface between 10 and 28 km. For each source, the data are recorded by a 'streamer' array (yellow line) with a maximum offset of 6 km.

Figure 10 Inverted parameters for the model from Fig. 9 (the tilt θ is estimated from the final LSRTM image): (a) V_{nmo}, (b) δ, (c) η and (d) θ.

obtain the initial field of this parameter from image-guided interpolation. Image-domain tomography (IDT) is performed using the cascaded iterative inversion scheme described above. Because the data are noise-free and produced with an acoustic modeling operator, matching filters are applied just to precondition the reverse-time migration (RTM) image.

At the first inversion stage, we update only V_{nmo} and δ. Because the image-power operator requires an accurate background model, the factor α in the objective function (equation
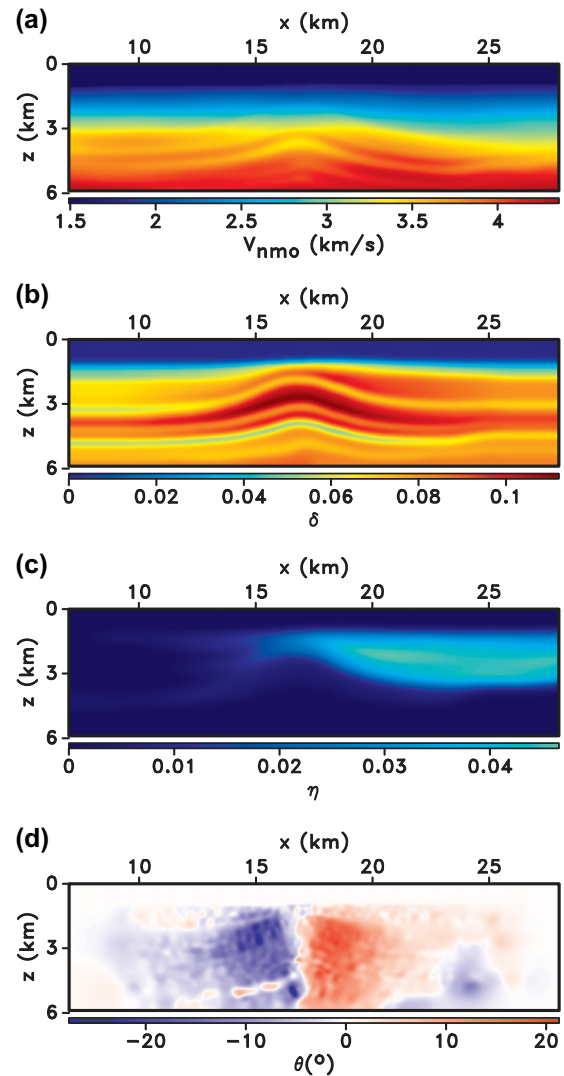
(4)) is initially set to 0.5, which emphasizes the differential semblance optimization term; the factor β is set to 0.85. Two iterations of IDT help refine the V_{nmo}- and δ-fields and reduce the objective function by about 50% (Fig. 10a,b). At the second stage, designed to update only η, we assign equal weights to the terms $\mathcal{J}_{DSO}$ and $\mathcal{J}_{IP}$ ($\alpha = 1$). Image-guided smoothing is applied to the η-gradient, which is set to zero in the water layer as well as below 3 km, where η cannot be reliably constrained within the available offset range.

One IDT iteration constrains the η-field on the right side of the anticline (Fig. 10c) and reduces the objective function by 10%. However, η is not well recovered to the left of the
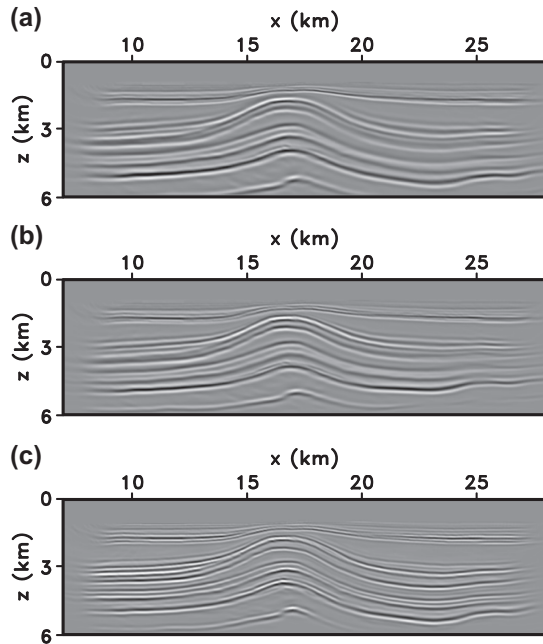
Figure 11 LSRTM images for the model from Fig. 9 computed with the (a) initial, (b) inverted, and (c) actual TTI parameters.

anticline due to the overestimated normal-moveout velocity in that area and relatively low effective values of η below the depth of 3 km. Repeating this two-stage inversion does not measurably reduce the objective function.

It should be mentioned that the IDT algorithm is not sufficiently sensitive to the TTI parameters below 3 km because the thick water layer and low-velocity overburden reduce the relative contribution of the deeper layers to the effective reflection traveltimes. Nevertheless, the updates in the TTI parameters improve the focusing of the migrated events in the shallow region (above 4 km) and produce a more accurate depth scale of the image (Fig. 11).

CONCLUSIONS

To extend image-domain tomography to tilted transversely isotropic (TTI) media, we derived a separable strongly anelliptic dispersion relation that accounts for the symmetry-axis tilt. The accuracy of that expression is sufficient for implementing the integral acoustic modelling operator and deriving the corresponding inversion gradients. We studied the extended-domain signatures of the parameters V_{nmo}, δ and η for a homogeneous TTI medium with the symmetry axis orthogonal to the reflector. In contrast to VTI media, the parameter δ not only changes the depth scale of the image but, along with V_{nmo}, contributes to the energy focusing for a wide range of reflector

dips and surface offsets. Errors in η cause only relatively weak linear (V-like) defocusing regardless of reflector dip, which is explained by the fact that η influences only long-spread (non-hyperbolic) moveout. The model-updating methodology was tested on a modified segment of the BP 2007 model. Although the initial model was highly inaccurate, the algorithm reconstructed the long-wavelength components of the parameters V_{nmo}, δ and η and noticeably improved the quality of the migrated section.

ORCID

Vladimir Li https://orcid.org/0000-0002-4453-371X
Hui Wang https://orcid.org/0000-0003-1877-0604

REFERENCES

Alkhalifah T. 1998. Acoustic approximations for processing in transversely isotropic media. *Geophysics* **63**, 623–631.

Behera L. and Tsvankin I. 2009. Migration velocity analysis for tilted transversely isotropic media. *Geophysical Prospecting* **57**, 13–26.

Chavent G. and Jacewitz C.A. 1995. Determination of background velocities by multiple migration fitting. *Geophysics* **60**, 476–490.

Claerbout J.F. 1992. *Earth Soundings Analysis, Processing Versus Inversion*. Blackwell Scientific Publication.

Du X., Fowler P.J. and Fletcher R.P. 2014. Recursive integral time-extrapolation methods for waves: a comparative review. *Geophysics* **79**, T9–T26.

Fomel S., Sava P., Vlad I., Liu Y. and Bashkardin V. 2013. Madagascar: open-source software project for multidimensional data analysis and reproducible computational experiments. *Journal of Open Research Software* **1**, e8.

Grechka V., Zhang L. and Rector J. 2004. Shear waves in acoustic anisotropic media. *Geophysics* **69**, 576–582.

Guitton A. 2017. Fast 3D least-squares RTM by preconditioning with nonstationary matching filters. SEG Technical Program, Expanded Abstracts, 4395–4399.

Hale D. 2009. Structure-oriented smoothing and semblance. CWP Project Review Report, 635, 1–10.

Li V., Tsvankin I. and Alkhalifah T. 2016. Analysis of RTM extended images for VTI media. *Geophysics* **81**, S139–S150.

Li V., Tsvankin I., Guitton A. and Alkhalifah T. 2017a. Acoustic VTI wavefield tomography of P-wave surface and VSP data. SEG Technical Program, Expanded Abstracts, 421–425.

Li V., Tsvankin I., Guitton A. and Alkhalifah T. 2018. Image-domain wavefield tomography for VTI media. *Geophysics* **84**, 1–80.

Li V., Wang H., Tsvankin I., Díaz E. and Alkhalifah T. 2017b. Inversion gradients for acoustic VTI wavefield tomography. *Geophysics* **82**, WA55–WA65.

Li Y., Biondi B., Clapp R. and Nichols D. 2016. Integrated VTI model building with seismic data, geologic information, and rock-physics modeling – part 1: theory and synthetic test. *Geophysics* **81**, C177–C191.

Pattnaik S., Tsvankin I., Wang H. and Alkhalifah T. 2016. Full-waveform inversion with reflected waves for 2D VTI media. SEG Technical Program, Expanded Abstracts, 413–418.

Plessix R.-E. 2006. A review of the adjoint-state method for computing the gradient of a functional with geophysical applications. *Geophysical Journal International* **167**, 495–503.

Sava P. and Alkhalifah T. 2012. Anisotropy signature in extended images from reverse-time migration. SEG Technical Program, Expanded Abstracts, 1–6.

Schleicher J. and Costa J.C. 2016. A separable strong-anisotropy approximation for pure qP-wave propagation in transversely isotropic media. *Geophysics* **81**, C337–C354.

Symes W.W. and Carazzone J.J. 1991. Velocity inversion by differential semblance optimization. *Geophysics* **56**, 654–663.

Tsvankin I. 2012. *Seismic Signatures and Analysis of Reflection Data in Anisotropic Media*, 3rd edn. Society of Exploration Geophysicists.

Tsvankin I. and Grechka V. 2011. *Seismology of Azimuthally Anisotropic Media and Seismic Fracture Characterization*. Society of Exploration Geophysicists.

Wang X. and Tsvankin I. 2013a. Ray–based gridded tomography for tilted transversely isotropic media. *Geophysics* **78**, C11–C23.

Wang X. and Tsvankin I. 2013b. Multiparameter TTI tomography of P-wave reflection and VSP data. *Geophysics* **78**, WC51–WC63.

Weibull W.W. and Arntsen B. 2014. Anisotropic migration velocity analysis using reverse-time migration. *Geophysics* **79**, R13–R25.

Zhan G., Pestana R.C. and Stoffa P.L. 2012. Decoupled equations for reverse time migration in tilted transversely isotropic media. *Geophysics* **77**, T37–T45.

Zhang Y. and Shan G. 2013. Wave-equation migration velocity analysis using partial stack-power maximization. SEG Technical Program, Expanded Abstracts, 4847–4852.

APPENDIX: SEPARABLE DISPERSION RELATION FOR TILTED TRANSVERSE ISOTROPY

Wavenumber rotation applied to equation (1) yields the "strongly anelliptic" approximation for the tilted transversely isotropic (TTI) dispersion relation. The symmetry-axis tilt θ can be separated from k_x and k_z by collecting all terms with

the same wavenumber components. Rotating the wavenumbers in equation (1) and keeping only the terms linear in the anisotropy coefficients, we obtain the following expression:

$$
\omega^2 = V_{P0}^2 \Big\{ (k_x^2 + k_z^2) + (2\varepsilon \cos^4\theta + 2\delta \sin^2\theta \cos^2\theta)\frac{k_x^4}{k_x^2 + k_z^2}
$$

$$
+ (2\varepsilon \sin^4\theta + 2\delta \sin^2\theta \cos^2\theta)\frac{k_z^4}{k_x^2 + k_z^2}
$$

$$
+ (4\varepsilon \sin 2\theta \cos^2\theta - \delta \sin 4\theta)\frac{k_x^3 k_z}{k_x^2 + k_z^2}
$$

$$
+ (4\varepsilon \sin 2\theta \sin^2\theta + \delta \sin 4\theta)\frac{k_x k_z^3}{k_x^2 + k_z^2}
$$

$$
+ (3\varepsilon \sin^2 2\theta - \delta \sin^2 2\theta + 2\delta \cos^2 2\theta)\frac{k_x^2 k_z^2}{k_x^2 + k_z^2} \Big\}, \qquad (A1)
$$

where V_{P0} is the P-wave symmetry-direction velocity and ε is Thomsen's anisotropy coefficient. In contrast to the result of Zhan *et al.* (2012), equation (A1) is consistent with the sign convention of the rotation matrix in equation 1.

For TTI media with relatively large values of the anisotropy coefficients, a more accurate approximation can be obtained by applying wavenumber rotation to the entire equation (1) and collecting all terms with the same wavenumber components:

$$
\omega^2 = L + \frac{2(\epsilon - \delta)V_{P0}^2}{(k_x^2 + k_z^2)^3}\Big\{ k_x^8 \cos^4\theta\,[\delta + \varepsilon + (\varepsilon - \delta)\cos 2\theta]\sin^2\theta
$$

$$
+ k_z^8 \sin^4\theta\,[\delta + \varepsilon + (\delta - \varepsilon)\cos 2\theta]\cos^2\theta
$$

$$
+ 2k_x^7 k_z \cos^3\theta\,[\delta - (2\delta + \varepsilon)\cos 2\theta + (\delta - \varepsilon)\cos 4\theta]\sin\theta
$$

$$
+ 2k_x k_z^7 \sin^3\theta\,[\delta + (2\delta + \varepsilon)\cos 2\theta + (\delta - \varepsilon)\cos 4\theta]\cos\theta
$$

$$
- \frac{1}{4}k_x^6 k_z^2 \cos^2\theta\,[-10\delta - 4\varepsilon + (17\delta + 3\varepsilon)\cos 2\theta
$$

$$
- 14\delta \cos 4\theta + 7\delta \cos 6\theta - 7\varepsilon \cos 6\theta]
$$

$$
+ \frac{1}{4}k_x^2 k_z^6 \sin^2\theta\,[10\delta + 4\varepsilon + (17\delta + 3\varepsilon)\cos 2\theta
$$

$$
+ 14\delta \cos 4\theta + 7\delta \cos 6\theta - 7\varepsilon \cos 6\theta]
$$

$$
+ \frac{1}{4}k_x^5 k_z^3 \sin 2\theta\,[5\varepsilon + (5\varepsilon - 9\delta)\cos 2\theta
$$

$$
+ 7\varepsilon \cos 4\theta - 7\delta \cos 6\theta + 7\varepsilon \cos 6\theta]
$$

$$
+ \frac{1}{4}k_x^3 k_z^5 \sin 2\theta\,[5\varepsilon + (9\delta - 5\varepsilon)\cos 2\theta
$$

$$
+ 7\varepsilon \cos 4\theta + 7\delta \cos 6\theta - 7\varepsilon \cos 6\theta]
$$

$$
+ \frac{1}{32}k_x^4 k_z^4\,[9\delta + 15\varepsilon + 20(\varepsilon + \delta)\cos 4\theta
$$

$$
+ 35(\delta - \varepsilon)\cos 8\theta]\Big\}, \qquad (A2)
$$

where L contains all terms on the right-hand side of equation (A1).